Calculation of photon energy deposition kernels and electron dose point kernels in water

Ernesto Mainegra-Hing[a)]
Ionizing Radiation Standards, National Research Council of Canada, Ottawa K1A OR6, Canada

D. W. O. Rogers
Physics Department, Carleton University, Ottawa K1S 5B6, Canada

Iwan Kawrakow
Ionization Radiation Standards, National Research Council of Canada, Ottawa K1A OR6, Canada

(Received 5 October 2004; revised 27 December 2004; accepted for publication 28 December 2004; published 17 February 2005)

Effects of changes in the physics of EGSnrc compared to EGS4/PRESTA on energy deposition kernels for monoenergetic photons and on dose point kernels for beta sources in water are investigated. In the diagnostic energy range, Compton binding corrections were found to increase the primary energy fraction up to 4.5% at 30 keV with a corresponding reduction of the scatter component of the kernels. Rayleigh scattered photons significantly increase the scatter component of the kernels and reduce the primary energy fraction with a maximum 12% reduction also at 30 keV where the Rayleigh cross section in water has its maximum value. Sampling the photo-electron angular distribution produces a redistribution of the energy deposited by primaries around the interaction site causing differences of up to 2.7 times in the backscattered energy fraction at 20 keV. Above the pair production threshold, the dose distribution versus angle of the primary dose component is significantly different from the EGS4 results. This is related to the more accurate angular sampling of the electron-positron pair direction in EGSnrc as opposed to using a fixed angle approximation in default EGS4. Total energy fractions for photon beams obtained with EGSnrc and EGS4 are almost the same within 0.2%. This fact suggests that the estimate of the total dose at a given point inside an infinite homogeneous water phantom irradiated by broad beams of photons will be very similar for kernels calculated with both codes. However, at interfaces or near boundaries results can be very different especially in the diagnostic energy range. EGSnrc calculated kernels for monoenergetic electrons (50 keV, 100 keV, and 1 MeV) and beta spectra (^{32}P and ^{90}Y) are in excellent agreement with reported EGS4 values except at 1 MeV where inclusion of spin effects in EGSnrc produces an increase of the effective range of electrons. Comparison at 1 MeV with an ETRAN calculation of the electron dose point kernel shows excellent agreement. © *2005 American Association of Physicists in Medicine*. [DOI: 10.1118/1.1861412]

I. INTRODUCTION

Many current treatment planning systems use convolution techniques for radiotherapy photon dose calculation. In the convolution or superposition method the dose is calculated by convolving the total energy released per unit mass with an energy deposition kernel (EDK).[1–5] It is also customary to use radial distributions of dose around isotropic point sources of electrons or beta emitters in an infinite water medium, so-called dose point kernels (DPKs), as the basis for many calculations of dose from various distributions of beta sources.[6–9] The essential difference is that energy deposition kernels have a preferred direction defined by the direction of the initial photon whereas the dose deposition kernels contain no angular information.

EDKs describe the way energy is spread away from the interaction site of the primary photon. EDKs can be obtained by deconvolving measured finite beam dose distributions,[10] but the technique has many drawbacks. Common practice is to calculate monoenergetic EDKs using analytical scatter-and-primary-dose models or Monte Carlo simulation. The analytical methods, however, fail to account fully for the three-dimensional nature of radiation transport and all relevant energy deposition processes. Monte Carlo simulation of energy deposition kernels is the only practical method for calculation that can consider all interactions of importance for the transport of secondary particles. In a similar way, most recent compilations for DPKs are based exclusively on Monte Carlo simulations.

Since the Monte Carlo simulation system EGS4 has been extensively used for the calculation of EDKs[5] and DPKs,[6] we have looked into the question of whether the new physics in the EGSnrc simulation system[11,12] produces kernels very different from previous ones calculated with EGS4. This could be of interest when using treatment planning software based on such kernels. For instance the Pinnacle^{3D} treatment planning system from ADAC Laboratories relies on energy deposition kernels originally calculated by Mackie *et al.*[5] using EGS4/PRESTA for photon energies between 100 keV and 50 MeV. To address the need for accurate determination of the dose in the diagnostic energy range, Alaei *et al.*[13] extended these calculations from 100 keV down to 20 keV.

Significant modifications were made to the EGS4 simula-

tion system in the improved version called EGSnrc, especially in electron and low-energy photon transport. Binding corrections for Compton interactions and relaxation processes after Compton and photoelectric interactions are now taken into account. The angular sampling of the electron–positron direction and the bremsstrahlung photons is now done in a more accurate and efficient way. An exact electron multiple scattering theory and a step-size independent electron transport algorithm are also among the improvements in EGSnrc (for more details see the EGSnrc manual[11] and the paper by Kawrakow[12]).

II. CALCULATIONAL DETAILS

The EGSnrc user-code EDKnrc was written[14] based on an EGS4 user-code, SCASPH, previously used for the calculation of monoenergetic energy deposition kernels.[5] EDKnrc simulates the interaction at the origin of a primary photon moving along the Z axis (ISOURC=0) or the emission from an isotropic point source of photons or electrons (monoenergetic or polyenergetic, ISOURC=1) and the corresponding energy spread in a phantom of arbitrary material. The energy deposited in voxels, defined by the intersection of spheres and cones, is scored using history-by-history statistics as discussed by Walters *et al.*[15] All relevant interaction processes are taken into account including Rayleigh scattering and atomic relaxations. The latter process will not affect significantly the energy deposition kernels in a low Z material such as water, but has been included here for the sake of completness. The XCOM cross section database[16] with updated photo-electric and pair production cross sections[17,18] (included in the current EGSnrc distribution) has been used to generate the PEGS4 data sets.

When calculating energy deposition kernels, one can also use the original photon source algorithm implemented in SCASPH, where photons are placed close to the origin in the first geometrical region and forced to interact there to avoid the singularity at the origin (ISOURC=2). However, in EDKnrc one can specify how close to the origin the initial interaction should occur.

The energy deposited in the geometry can be separated into different contributions from each photon scattering order (e.g., primary, first scatter, second scatter, multiple scatter and radiative). For electrons, the deposited energy can be split into primary and radiative contributions.

II.A. Photons

Incident photons were forced to interact at the centre of a 60 cm radius water phantom and their secondary particles were followed through the geometry. As in earlier EGS4 calculations, the phantom was divided up by 48 cones (each separated by a polar angle of 3.75°) and 24 radial shells.[5] The distance between the radial boundaries was smaller near the origin, increasing with distance from 0.05 cm in the first shell up to 10 cm near the edge of the phantom. This spatial arrangement was chosen because energy deposition is highest near the site of interaction and the dose gradient is larger there. Photons and electrons were followed until their energies fell below a cut-off energy of 1 keV.

Energy depostion kernels for a given category (e.g., total, primary, first scatter, etc.) are defined as the fractional amount of the photon energy deposited in a scoring voxel:

$$\epsilon(i,j) = \frac{E_{\mathrm{dep}}(i,j)}{N_0 h\nu_0}, \tag{1}$$

where $E_{\mathrm{dep}}(i,j)$ is the energy deposited in voxel i,j,N_0 is the number of primary photons, and $h\nu_0$ is the primary photon energy. Summing $\epsilon(i,j)$ over the whole sphere gives the energy fraction for a given category.

Energy deposition kernels for monoenergetic photons in water were calculated for energies from 15 keV up to 50 MeV. In Sec. III a comparison with previous EGS4 calculations by Mackie *et al.*[5] will be presented and analyzed. The energy deposition kernels obtained using EGSnrc are available upon request from E.M.H.

Algorithm for primary photon interaction. When forcing a photon interaction at the origin of the coordinate system where all cones have a common point, a singularity exists since this point belongs to all cones and therefore to all geometrical regions surrounding the origin. The forcing algorithm implemented in EGS4 SCASPH makes use of a trick to overcome this. The primary photons are shifted by a small distance (10^{-6} cm) into the first region in the direction the primary photon is moving. This assures that the particles are really in a defined region when the interaction occurs. Moreover, to avoid the rare event of a particle moving into the origin, every time a particle intersects either a sphere or a cone, the distance to that boundary is increased by 10^{-6} cm to ensure that the particle penetrates into the new region.

This approximation can be the source of potential artifacts in the calculation of dose distributions as will be shown in Sec. III. For instance, charged particles generated after a primary interaction with an energy below the transport cut-off energy, deposit their energy on the spot, i.e., in the first region, overestimating the energy depostion there. While the numerical patches used to avoid the singularity at the origin might work for a given combination of computer architecture and compiler, it might introduce significant errors in other configurations.

A new algorithm was implemented in EDKnrc which selects the type of interaction the primary photon undergoes and distributes the secondary particles after the interaction into the proper region according to their direction after the interaction. Initially the primary photon and its secondaries sit right at the origin, i.e., no approximation is made about the real position of the particles. If a charged particle is going to deposit its energy on the spot, it will do it in the correct region and not in the first region as would be the case with the previous algorithm.

When taking into account relaxation processes after a Compton or photoelectric interaction, particles with energies above the transport cut-offs (ECUT and PCUT) are placed on the stack and the energy of subthreshold particles is deposited locally on regions surrounding the origin which are

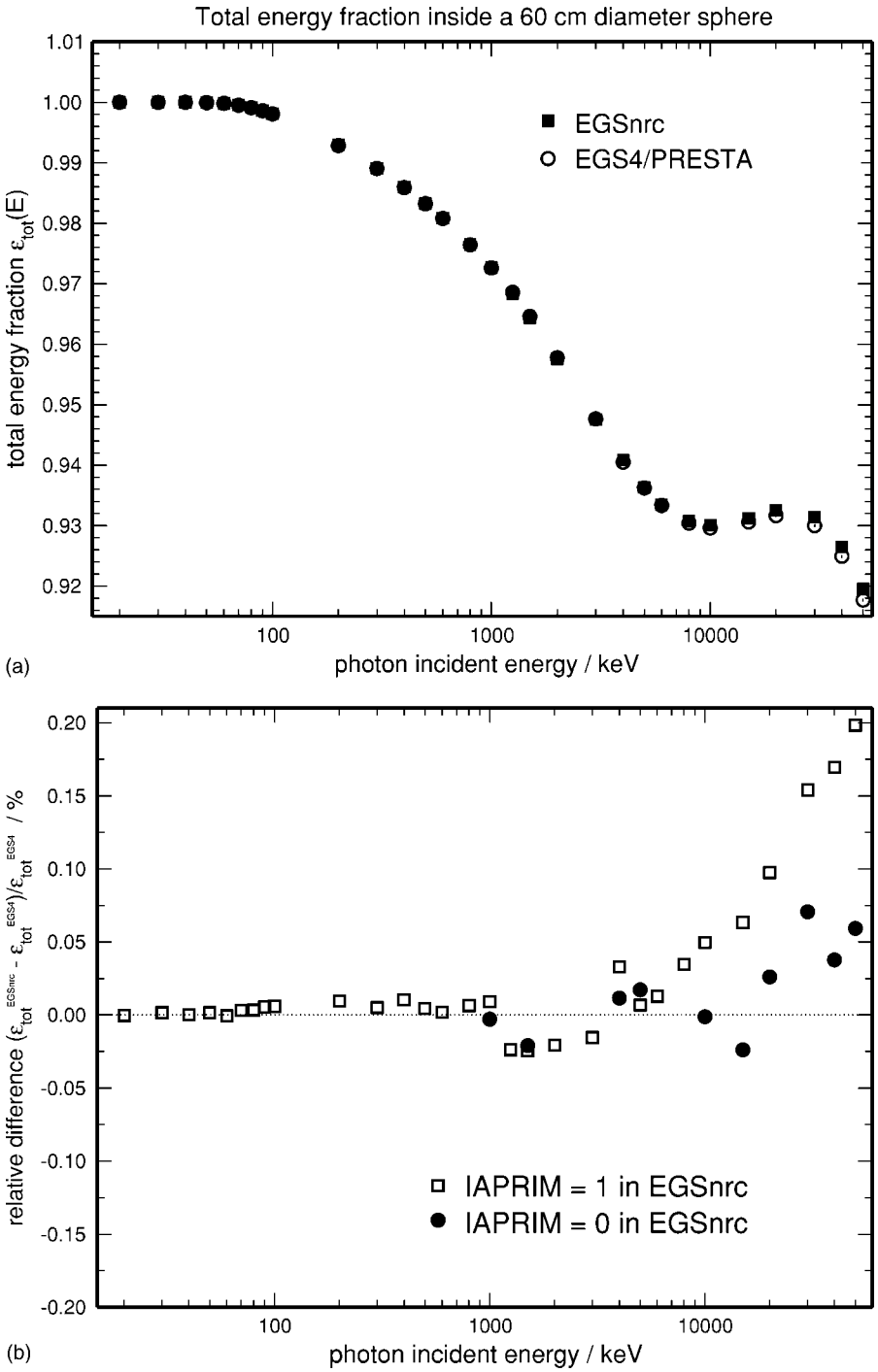

FIG. 1. Upper panel shows the total energy fraction for monoergetic photons (15 keV–50 MeV) calculated with EDKnrc (squares) using IAPRIM=1 and SCASPH (circles). Lower panel: Relative difference in the total energy fraction for the same two cases (squares) and also showing the result if the same radiative stopping powers are used in the EGSnrc calculations as in the EGS4 calculations (IAPRIM=0). Statistical error for the energy fractions is less than 0.05% (1σ standard deviation).

randomly selected based on their solid angle. Only shell vacancies above 1 keV are treated due to lack of low-energy data in the EGSnrc system.[11]

II.B. Electrons

The energy deposited in spherical shells has been scored to obtain dose point kernels in water for 50 keV, 100 keV, 200 keV, and 1 MeV monoenergetic electron point sources and for ^{32}P and ^{90}Y beta sources. To model the beta sources we have taken the spectra from the ICRU Report 56.[19] Electrons and secondary photons are followed until they leave the geometry or their energy falls below a 1 keV energy cut-off.

The dose distribution is converted into a dimensionless quantity as suggested by Cross[7] to become a slowly varying quantity with energy, making interpolation in energy more accurate with relatively wide energy intervals. This dimensionless quantity is defined as

$$j(r/r_{\mathrm{CSDA}},E) = 4\pi\rho r^2 D(r,E) r_{\mathrm{CSDA}}/E \qquad (2)$$

with r being the radial distance to the middle of the spherical shells, r_{CSDA} the nominal CSDA range, ρ the density of the

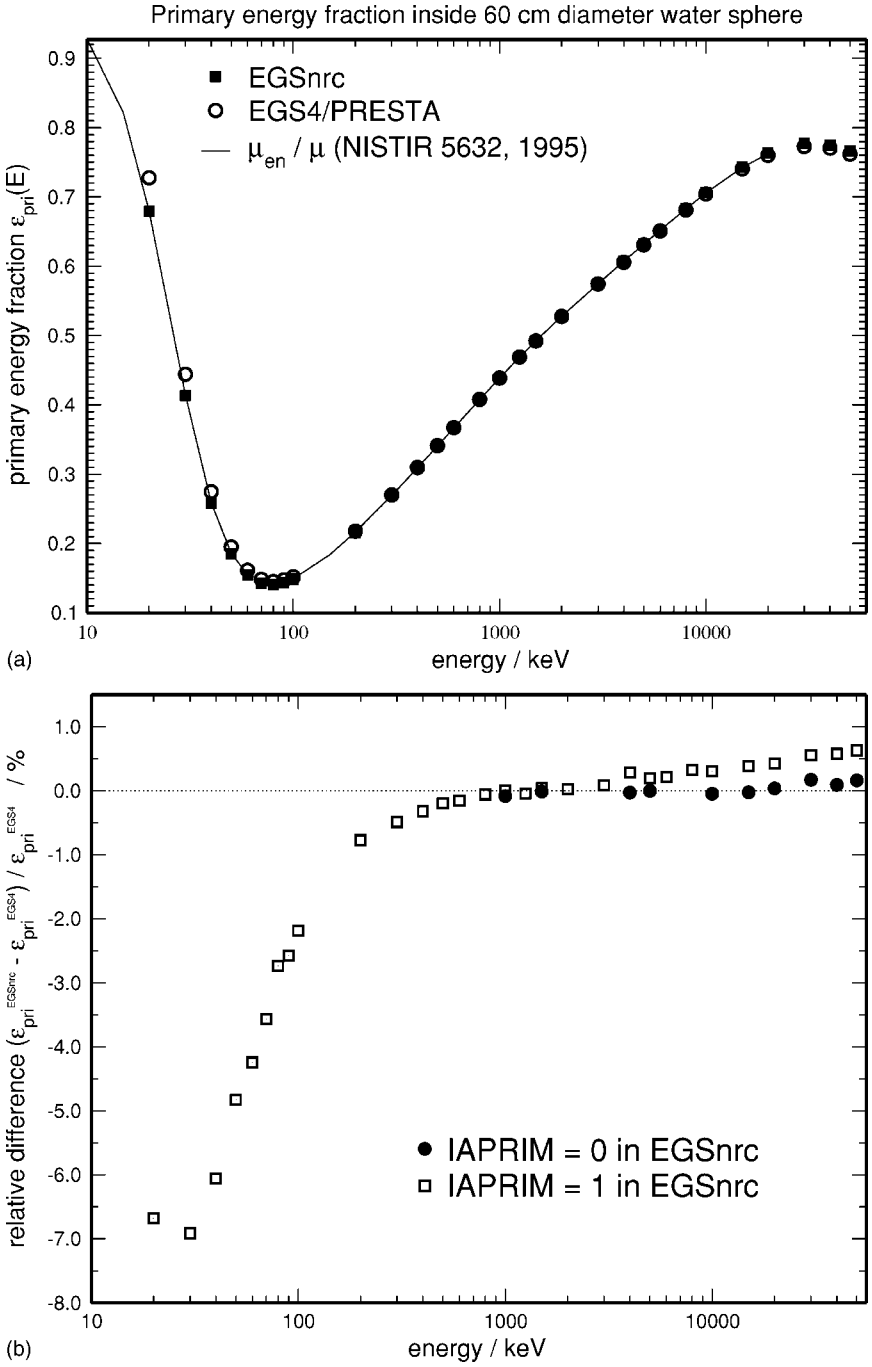

FIG. 2. Upper panel: Primary energy fraction as function of incident photon energy calculated with EDKnrc (squares) and SCASPH (circles) and the theoretical estimate, μ_{en}/μ taken from the data compilation by Hubbell and Seltzer (Ref. 28) 1995 (triangles). Lower panel: Relative difference in percent between the EDKnrc and SCASPH energy primary fractions (squares). Note that setting IAPRIM to 0 reduces the differences at high energies (circles). Statistical error for the energy fractions is less than 0.05% (1σ standard deviation).

medium, and $D(r,E)$ the dose per incident particle at distance r. The quantity defined in Eq. (2) represents the fraction of emitted energy that is deposited in a spherical shell of scaled radius r/r_{CSDA} to $r/r_{\mathrm{CSDA}}+d(r/r_{\mathrm{CSDA}})$.

In these calculations we have taken r_{CSDA} values from the NIST web database ESTAR which generates stopping powers and ranges for electrons which are the same as those tabulated in ICRU Report 37[20] (ICRU, 1984) for 72 materials at a standard grid of 81 kinetic energies between 10 keV and 1000 MeV.

Other authors use different scaling distances instead of the CSDA range to define this scaled dose kernel. For example, Simpkin and Mackie[6] in their work chose both the CSDA range and X_{90}, the radius of the sphere within which 90% of the emitted energy is absorbed.

To obtain the dose point kernel around an isotropic point source of electrons, a spherical water phantom was divided into 22 spherical shells each of thickness 0.05 r_{CSDA}. This selection was made for comparison with the results by Cross who used this thickness. However, one can use an arbitrarily small resolution in the user-code EDKnrc. Dose point kernels for ^{32}P and ^{90}Y beta particles were calculated with a 5 and 1 μm resolution, respectively, and scaled by X_{90} for comparison with the results by Simpkin and Mackie.

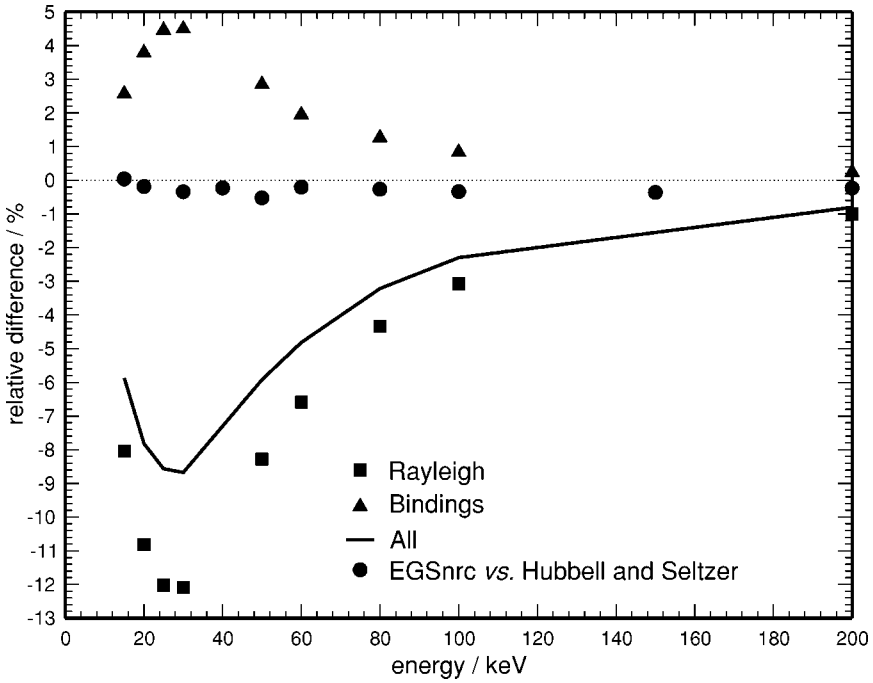

FIG. 3. Relative differences in calculated primary energy fractions values compared to a base case using the same photon physics as EGS4 and then adding Rayleigh and/or bound Compton scattering. Also included is a comparison of our best calculated EGSnrc estimate for the primary energy fraction to the μ_{en}/μ values taken from the 1995 data compilation by Hubbell and Seltzer (Ref. 28). One sigma standard deviation for the primary energy fractions is less than 0.05%.

III. RESULTS

III.A. Photon energy deposition kernels

Energy deposition kernels were obtained for photon energies from 15 keV up to 50 MeV using the EGSnrc Monte Carlo simulation system. Our calculations have been compared with the results by Mackie *et al.*[5] and Alaei *et al.*[13] Both groups of authors used the EGS4 user-code SCASPH, but the 1988 calculations by the first authors cover only the energy range from 100 keV to 50 MeV. In 1999 the latter authors completed the initial calculations by extending them from 100 keV down to 20 keV.

Below about 80 keV the total energy deposition fractions are unity (see Fig. 1 upper panel), i.e., all energy is deposited in the 60-cm-diam water sphere. The total energy fractions start decreasing with increasing energy above 80 keV since radiation starts escaping the phantom. A comparison with previous EGS4 calculated kernels in the lower panel of Fig. 1 shows that the total energy fraction is practically the same within uncertainties for both calculations except at energies above 10 MeV were a maximum difference of 0.2% at 50 MeV is obtained. This suggests that for homogeneous, infinte phantoms, dose calculations for broad beams using convolution methods with either energy deposition kernels would produce similar results within the above stated difference.

The small differences encountered at high energies can be somewhat accounted for by the difference in the empirical scaling factor used when generating the bremsstrahlung cross section data sets with PEGS4 (the IAPRIM flag, see stars in lower panel of Fig. 1). In the original EGS4 implementation this empirical factor is based on data provided by Koch and Motz[21] (IAPRIM=0). But a different selection of this scaling factor was implemented in the EGS4 data preparation package PEGS4 by Rogers *et al.*[22] to ensure the radiative stopping powers calculated by PEGS4 match those in the ICRU Report 37[20] (IAPRIM=1).

Primary energy fractions are the fraction of the total incident energy which is deposited by the electrons set in motion by the initial photon interaction. The values calculated using the EGSnrc and EGS4 user-codes EDKnrc and SCASPH, respectively, are shown in the upper panel of Fig. 2 together with the ratio of the energy absorption coefficient, to the total attenuation coefficient, μ_{en}/μ (triangles), which for energy conservation reasons should be equal to the primary energy fraction deposited in the phantom. The EGSnrc calculated primary energy fractions differ from the EGS4 calculations at low energies as can be observed from the squares in lower panel of Fig. 2 where a maximum discrepancy of 7.0% is found at 30 keV. In the higher energy range this difference is much smaller but reaches 0.6% at 50 MeV. As in the case for the total energy fractions, if one sets IAPRIM to 0, the differences in the high energy range are reduced to less than 0.2% (stars).

To understand the large differences in the primary energy fraction at low energies, several calculations were performed. Unlike our reported results, our base case for these investigation is an EGSnrc calculation using the same photon transport parameters as in earlier EGS4/PRESTA calculations. This means, binding corrections, Rayleigh scattering and photo-electron angular sampling are not included in the base case. We then turn on each of the relevant processes individually (Rayleigh scattering and Compton binding corrections) and subsequently run a calculation with both processes turned on.

The primary energy fractions for the three different cases were compared to the base case and the relative differences

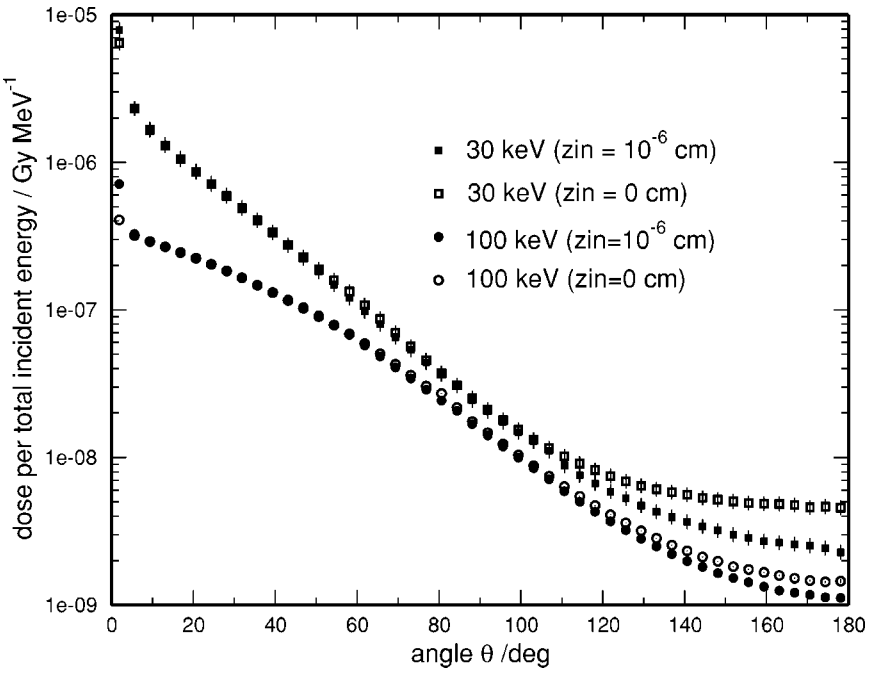

FIG. 4. Dose distribution vs angle around the primary interaction site (inside first sphere, $r=0.05$ cm) for 30 keV (squares) and 100 keV photons (circles). Closed squares and circles were obtained forcing the primary photon to interact at 10^{-6} cm from the origin. Open squares and circles are calculations using the new forcing algorithm at the origin. Differences observed are caused by the intial forcing algorithm artifact. These calculations were all done with ESTEPE $=0.02$, and Compton binding corrections, Rayleigh scattering and photoelectron angular sampling turned off to isolate the artifacts caused by the forcing algorithm.

are shown in Fig. 3. One can see that including Compton binding corrections (triangles) increases the primary energy fraction with a maximum difference of 4.5% at 30 keV. On the other hand, when only Rayleigh scattering is included, the number of interactions increases, but the primary energy deposited remains the same. Thus the primary energy fraction is reduced up to 12% at 30 keV, which is exactly the fraction $\sigma_{\mathrm{Ray}}/\sigma_{\mathrm{tot}}$ at this energy. Finally, when both Rayleigh and Compton binding corrections are included the net difference is given by the solid line in Fig. 3 with a maximum discrepancy of 8.6% at 30 keV. The 1.6% difference with the value from Fig. 2 at this energy is a direct consequence of using different cross-section data compilations in this work (Berger and Hubbell[16]) and in Mackie *et al.*[5] (Storm and Israel[23]).

Mackie *et al.*[5] reported a good agreement between the primary energy fraction and the ratio μ_{en}/μ taken from the data compilations by Hubbell[24–26] in the energy range from 100 keV up to 10 MeV. Alaei *et al.*[27] also compared their primary energy fraction with this ratio in the energy range between 20 and 100 keV, reporting an average difference of 1.03%. Both group of authors did not include Rayleigh scattering in their calculations (although they could have), which is the major source of discrepancy with the current calculations. We have included here a similar comparison in Fig. 3 for energies between 15 and 200 keV of our calculated primary energy fractions and μ_{en}/μ values from the more recent 1995 data compilation by Hubbell and Seltzer.[28] Unlike earlier data compilations, their values include Rayleigh scattering and Compton binding effects. The agreement of our Monte Carlo calculated primary energy fractions with these values is better than 0.5% (circles).

As already seen above, the major differences can be found at very low energies were the inclusion of Compton binding effects and Rayleigh scattering have their largest impact on the kernels, and at energies above the pair production threshold. In the following sections we will discuss the impact of the artifacts caused by the forcing algorithm and the electron transport algorithm and the improvements in EGSnrc on the energy deposition kernels. Although in some cases we will be reporting EGS4-like calculations with EGSnrc in an attempt to better understand the differences found between both calculations, this can never be a faithful reproduction of EGS4 since EGSnrc always uses a new electron multiple scattering theory, a more accurate path length correction and corrected bremsstrahlung sampling routines. Moreover, EGSnrc has fixed the fictitious cross-section problem and handles energy loss more accurately.[12]

III.A.1. Artifacts due to primary interaction forcing algorithm and electron transport algorithm

As mentioned earlier, the algorithm for forcing the first photon interaction in the EGS4 user-code SCASPH can potentially produce unrealistic artifacts, since electrons generated

TABLE I. Fraction of deposited energy in the innermost sphere (sphere surrounding interaction site) by primary photon interactions due to subthreshold events. It includes all events that produce secondary particles below the transport cut-off energies ECUT (0.512 MeV) and PCUT (0.001 MeV).

Energy (MeV)	Energy fraction (%)
0.015	3.40
0.030	1.95
0.100	0.81
1.000	0.10
10.000	0.09
20.000	0.06
50.000	0.02

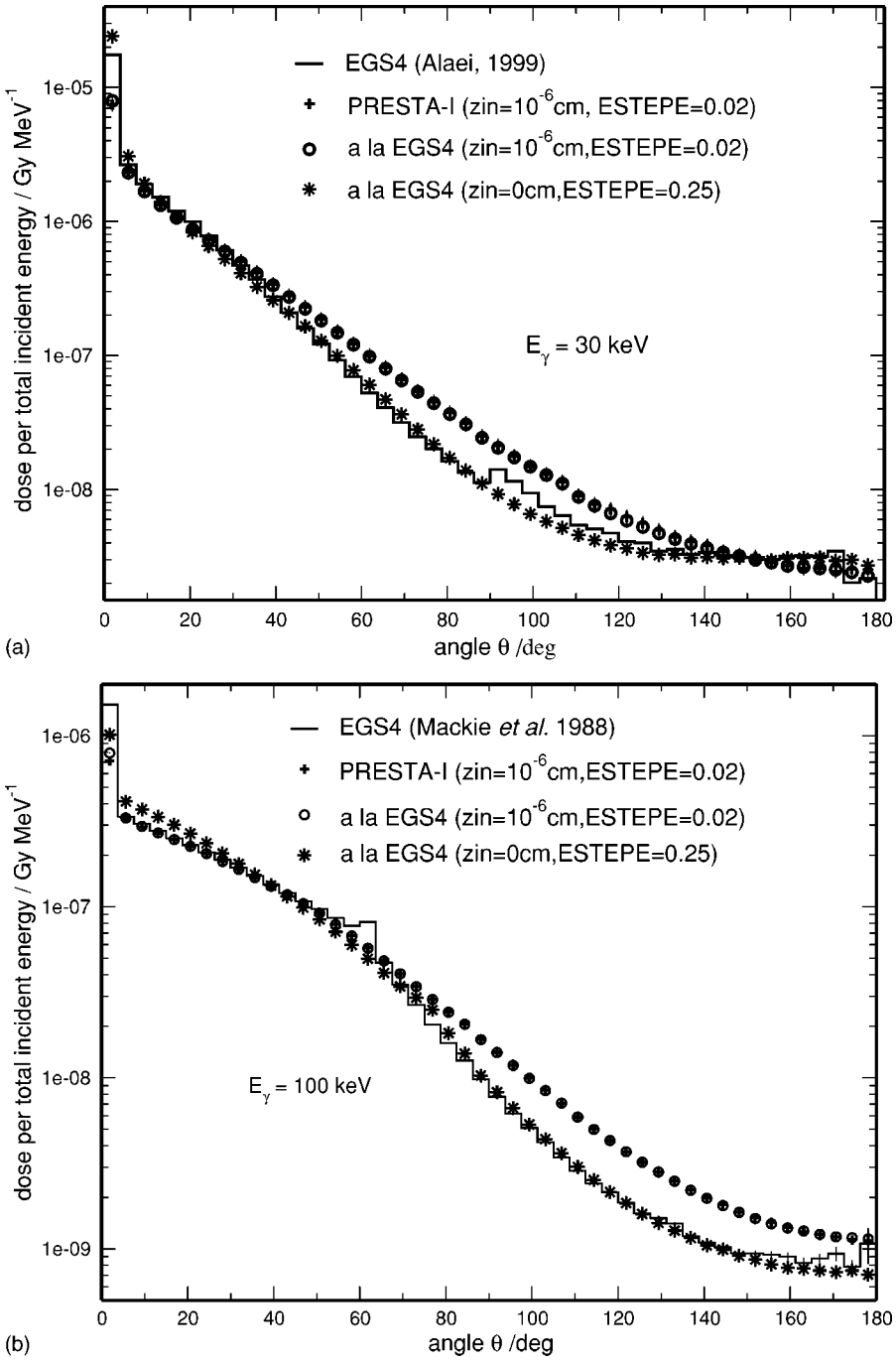

FIG. 5. Dose distribution vs angle around the primary interaction site (innermost sphere) for 30 keV (upper panel) and 100 keV photons (lower panel). Histograms are EGS4/PRESTA calculations by Alaei *et al.* (Ref. 13) and Mackie *et al.* (Ref. 5). Crosses represent calculations mimicking PRESTA-I behavior, and circles and stars are EGS4-like calculations. Since the same initial photon forcing algorithm is used in the first three cases, the observed differences are caused by the different electron transport.

during primary photon interactions, with kinetic energies below the cut-off energy ECUT, will dump their kinetic energy on the spot, i.e., in the initial geometrical region. This effect can be observed in Fig. 4 where the dose per incident energy deposited by 30 and 100 keV photons in the innermost water sphere is plotted as a function of angle. The closed symbols correspond to EGSnrc calculations forcing the primary photon interaction at 10^{-6} cm from the origin in the first geometrical region and the open symbols are EGSnrc calculations with the new forcing algorithm at the origin. One can see that forcing the primary photons to interact away from the origin overestimates the energy deposition in the directly forward angular bin and underestimates the energy deposition at large back angles. This artifact only affects the energy deposition of low energy photons in the inner most sphere, and disappears at larger distances from the origin. For 15 keV photons 3.4% of the energy deposited by primary particles in the first sphere is due to subthreshold events and for 100 keV photons this fraction is only 0.8%. Table I shows the fraction of energy deposited in the first sphere due to sub-threshold events at different energies.

The angular energy deposition will be affected by the new electron transport algorithm and the new multiple scattering theory used in EGSnrc. This will be true especially in the inner most sphere where secondary electrons can be scattered into the neighbor regions surrounding the interaction site.

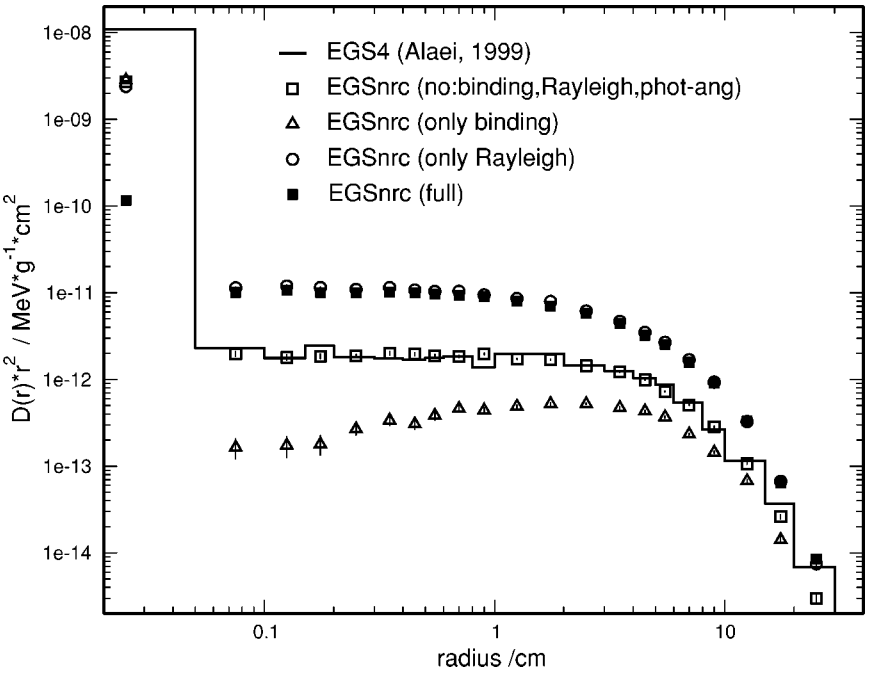

FIG. 6. Radial dose distribution times r^2 for 30 keV photons along the direction of the primary photon (first angular bin 0°–3.75°). EGSnrc and EGS4 results are represented by closed squares and a histogram, respectively. Also included in the graph are calculations without any low energy photon transport improvements (open squares), with only binding corrections (triangles), and with only Rayleigh scattering (circles).

Figure 5 shows the energy deposition versus angle inside the first sphere for 30 and 100 keV photons calculated with EGSnrc mimicking PRESTA-I (crosses) and EGS4 behavior (circles), and with EGS4 (histograms). All these calculations use an ESTEPE of 0.02. Both EGSnrc calculations are very similar and the difference with the previous EGS4/PRESTA calculations is caused only by the different electron transport in EGS4 and EGSnrc. One can also see that an EGS4-like EGSnrc calculation with ESTEPE=0.25 and the new forcing algorithm (stars) reproduces better the calculations reported by Mackie *et al.* and Alaei *et al.* For information on how to mimic EGS4 and EGS4/PRESTA behavior the user is referred to PIRS-701, the EGSnrc manual,[11] Secs. 3.4.2.i and 3.4.2.ii.

III.A.2. Effect of changes at low energies

In Sec. III A we saw that maximum discrepancies in the primary energy fraction are found at 30 keV due to Rayleigh scattering and Compton binding effects. It is precisely at 30 keV that the Rayleigh scattering cross section for water has its maximum value which reduces the primary energy fraction by as much as 12%. The photo-effect ceases to be

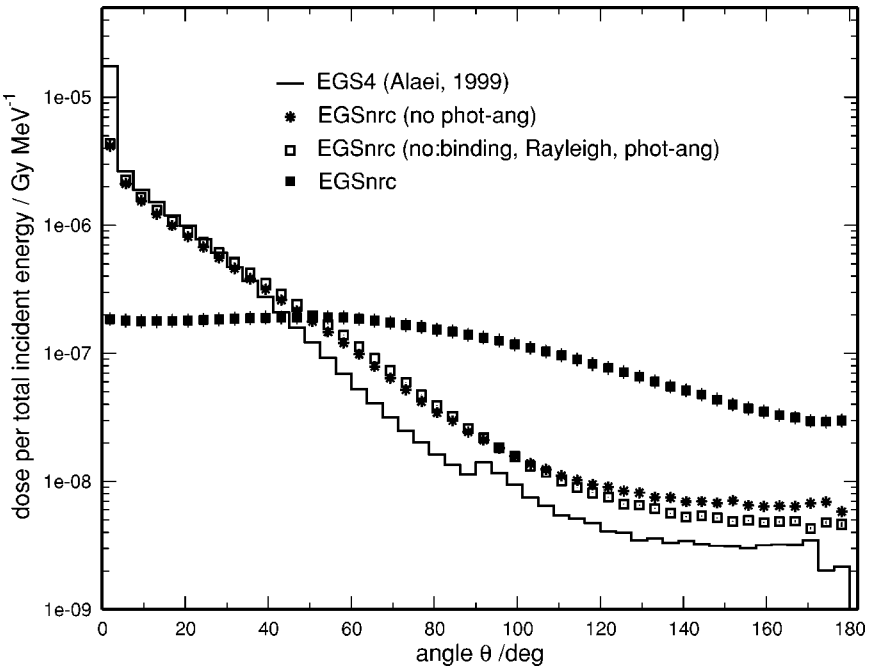

FIG. 7. Dose in the first scoring sphere vs angle for 30 keV photons. Full EGSnrc and EGS4 results are represented by closed squares and a histogram, respectively. Included in the graph are calculations without any low-energy photon transport improvements (open squares), and with only photo-electron angular distribution sampling switched off (stars). The big difference between the full EGSnrc calculation and the other EGSnrc calculations is caused by the photo-electron angular distribution sampling.

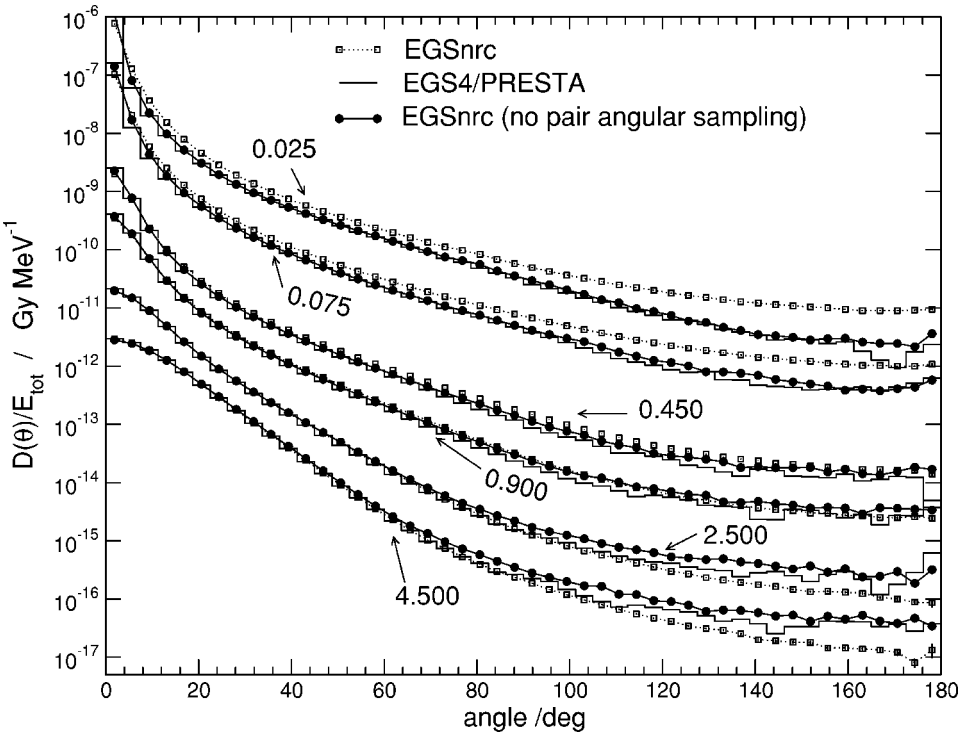

FIG. 8. Primary dose distribution for 20 MeV photons as function of angle for different distances. As can be seen, the EGSnrc calculation without pair angular sampling (closed circles) better reproduces the EGS4/PRESTA results of Mackie *et al.*—Ref. 5 (histograms).

the dominant process in water also at around 30 keV and the Compton scattering process takes over. Because binding effects are more important for small energy transfers, one can find the maximum effect of this correction also at around 30 keV.

The dose point kernel along the direction of the primary 30 keV photons, i.e., $\theta=0°$ (see Fig. 6) obtained with EGSnrc considering all the low-energy processes available in the system looks very different to the one calculated using EGS4/PRESTA. The scatter component of the dose is five to three times larger in the EGSnrc results because of the inclusion of Rayleigh scattering which acts as a source of scattered photons with practically the initial photon energy. Binding corrections cause the scatter component to be depressed since they reduce the number of primary interactions by 7.5% at 30 keV. If one neglects binding effects and Rayleigh scattering the EGSnrc calculations agree well with the EGS4/PRESTA calculations except in the first radial bin due to the artifact produced by the forcing algorithm used in SCASPH. There is also a very large difference (30 times) in this first radial bin between the full EGSnrc calculation and the other EGSnrc results shown in the graph. As will be seen in the following, this is caused by the redistribution of the energy deposited by primaries when the photo-electron angular sampling is switched on as is the case in the full EGSnrc calculation.

The angular distribution of the dose deposited in the innermost sphere for 30 keV electrons is shown in Fig. 7. An EGSnrc calculation without Rayleigh scattering, binding corrections and photo-electron angular distribution is very similar to the EGSnrc calculation without the sampling of the photo-electron angle. Moreover, both calculations show the same trend as the EGS4/PRESTA values although some noticeable differences can be seen probably due to the artifacts mentioned previously in Sec. III A 1. As soon as the photo-electron angular distribution sampling is switched on, a less steep angular dose profile is obtained.

In EGS4, the direction of the photo-electron is the same as the direction of the interacting photon by default, which is a good approximation at high energies. This can be changed to sampling the direction of the photo-electron from the Sauter distribution[29,30] by setting the region dependent array variable IPHTER to 1 in desired regions. Version 4 of the EGS4 user-code SCASPH does not allow changing this flag, i.e., the EGS4 calculations of energy deposition kernels with SCASPH reported in the literature[5,27] use the EGS4 default of not sampling the photo-electron direction. EGSnrc on the other hand samples by default the photo-electron direction as implemented by Bielajew and Rogers.[30] This sampling of the photo-electron direction causes a redistribution of the energy deposited around the primary interaction site compared to the results obtained with the EGS4 user-code SCASPH. At high energies, electron multiple scattering would "wash out" this angular distribution, while at the same time, the photo-electric effect contribution would become less important.

III.A.3. Effect of changes at higher energies

Radial and angular energy deposition kernels for 1 MeV photons calculated with the EGSnrc user-code EDKnrc were

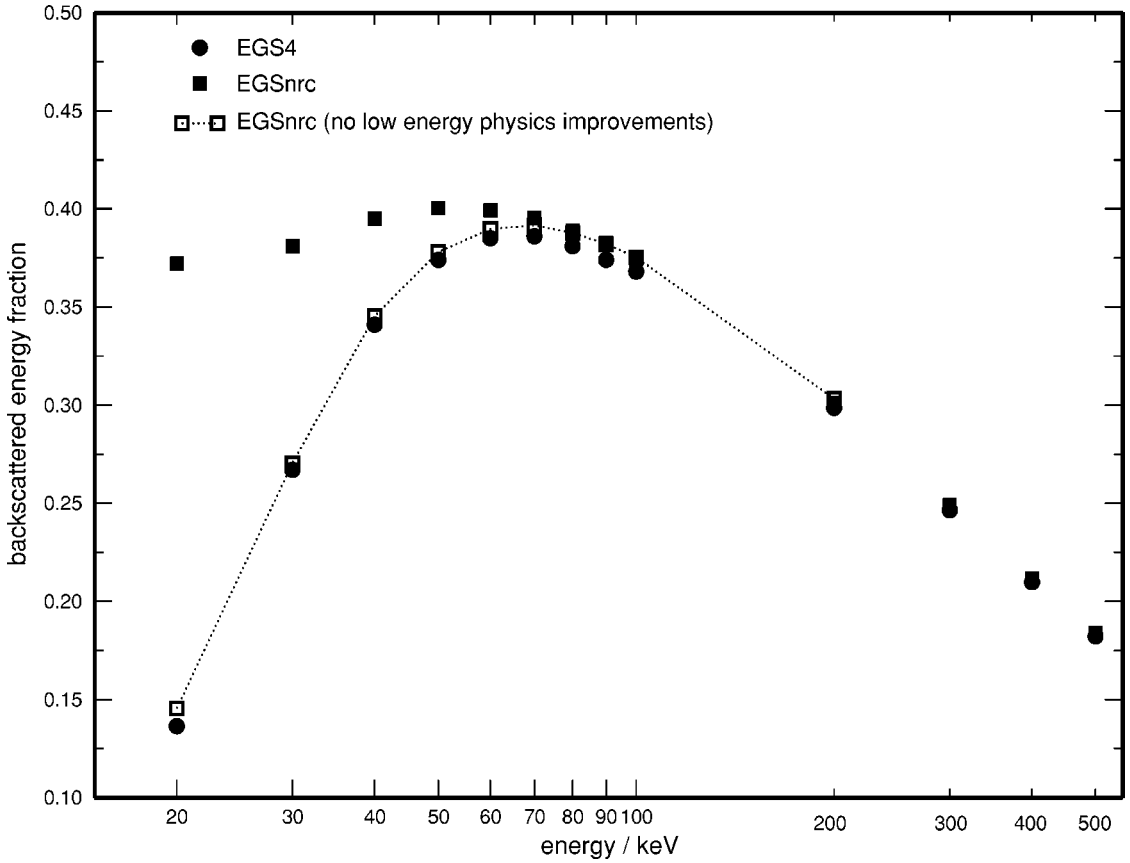

FIG. 9. Comparison of the backscattered energy fraction in water as function of photon energy calculated with EGS4/PRESTA by Alaei *et al.*—Ref. 27 ($E<100$ keV) and by Mackie *et al.*—Ref. 5 ($E>100$ keV) with our EGSnrc calculations with (closed circles) and without (open circles) the low energy improvements for photon transport. Backscattered energy fractions are obtained by summing the energy fraction deposited in the angular interval from 90° to 180°.

compared to the EGS4/PRESTA results and a good agreement was obtained except at back angles where the observed differences are small compared to the large differences found in the diagnostic energy range and might be caused by statistics.

Above the pair production threshold one starts observing differences in the primary dose component at large angles. These differences increase with increasing energy and Fig. 8 illustrates this for 20 MeV photons. The angular dose distributions at different distances from the interaction point are shown for the EGS4 calculation by Mackie *et al.*[5] (histogram) and a full EGSnrc calculation (open squares). Very close to the interaction point, the dose obtained with EGSnrc is larger than with EGS4. Moving away from the interaction point, both results get closer to each other and then at large angles grows apart again, this time the EGSnrc results are lower than the EGS4 calculations. We have found that these differences are caused by the different ways the electron(positron) direction with respect to the direction of the incoming photon is obtained in EGSnrc and EGS4. The closed circles in Fig. 8 represent an EGSnrc calculation with pair angular sampling switched off using a fixed angle approximation ($\theta_{\pm}=m/k$) in the same way as in EGS4. This setting makes the agreement with the EGS4 calculations better, especially at distances close to the interaction point.

III.A.4. Influence on dose estimate

Will the differences found in the energy deposition kernels affect the dose estimate in treatment planning systems using convolution methods? For the ideal case of an infinite homogeneous medium irradiated by a broad beam, if the convolution kernels are used in conjunction with the same cross sections used for their calculation to estimate the terma, no differences should be seen in the dose estimate. For instance, the 4.6% increase in the primary energy deposition fraction at 30 keV when using binding corrections cancels out with the reduction of the number of interactions needed to obtain the same energy deposition, which also amounts to 4.6%. In a similar manner, the 12% reduction found in the primary energy fraction at this energy when including Rayleigh scattering would cancel with the corresponding increase in the total cross section by the same amount.

However, in the presence of interfaces, boundaries, and inhomogeneities, results using either EGS4 or EGSnrc calculated energy deposition kernels can be very different. As an example, we have compared the backscattered energy frac-

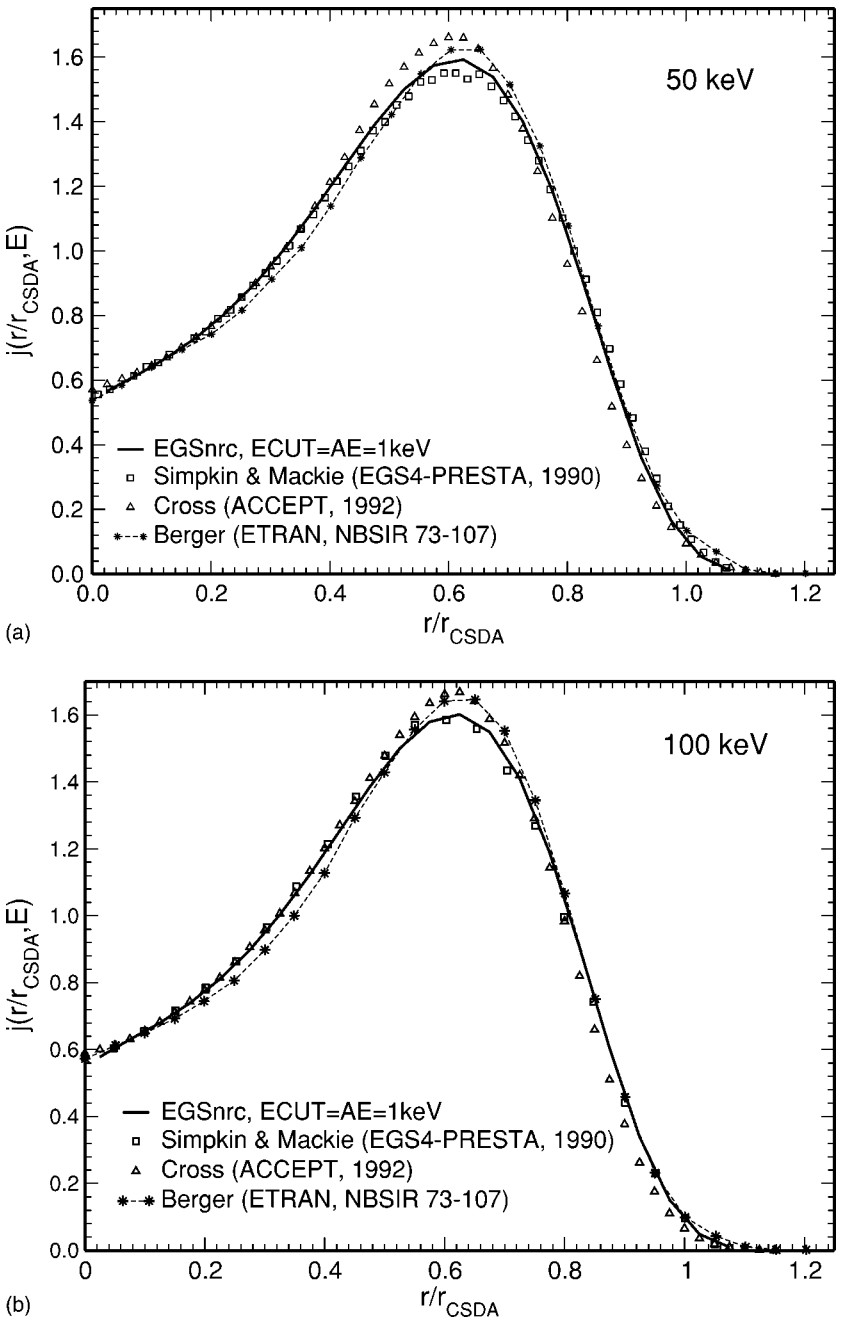

FIG. 10. Comparison of EGSnrc calculated dose point kernels for 50 keV (upper panel) and 100 keV (lower panel) electrons with EGS4 (Simpkin and Mackie—Ref. 6), ACCEPT (Cross—Ref. 7) and ETRAN (Berger—Ref. 31) calculated values.

tions obtained by summing the energy fraction deposited in the angular interval from 90° to 180°. The EGS4 and EGSnrc backscattered energy fractions are shown in Fig. 9 as circles and closed squares, respectively. At energies above 100 keV both energy fractions are almost the same. Below this energy, large differences appear and EGSnrc predicts 2.7 times more backscattering than the EGS4 value at 20 keV. This may have a large impact when, for example, one is interested in calculating the dose on or very close to a surface for low energy photon beams.

III.B. Monoenergetic beta dose kernels

Several dose point kernels were calculated for isotropic monoenergetic electron sources ranging from 50 keV up to 3 MeV. For these calculations the energy deposited in each of the spherical shells was scored. Discrepancies encountered in the dose point kernels among different Monte Carlo codes will be caused by the differences in the methods of sampling energy losses and angular deflections.

Figure 10 includes a comparison of the dimensionless quantity $j(r/r_{\mathrm{CSDA}},E)$ obtained using the EGSnrc user-code EDKnrc with several calculations reported in the literature for 50 keV (upper panel) and 100 keV (lower panel) monoenergetic electron sources. A fairly good agreement with the EGS4 calculation by Simpkin and Mackie[6] can be found at both energies. The curves calculated by Berger[31] using the 1973 version of ETRAN and by Cross *et al.*[7] with the 1988 version of ITS/ACCEPT code, a derivative of ETRAN, are also

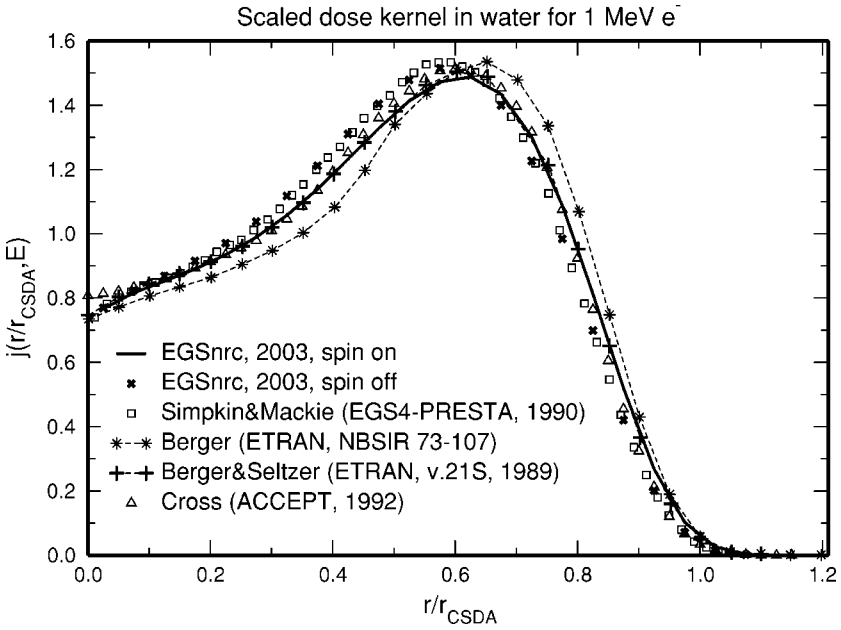

FIG. 11. Comparison of EGSnrc calculated dose point kernels for 1 MeV electrons with calculated values using EGS4 (Simpkin and Mackie—Ref. 6), ACCEPT (Cross—Ref. 7), an early version of ETRAN (Berger—Ref. 31), and the corrected ETRAN version (taken from Ref. 6) calculated values.

shown. The two data sets differ from the EGSnrc and EGS4 calculations by a few percent which can be expected from the fundamental differences in the codes.

Prior to 1986, the sampling of the Landau energy-loss straggling theory used in ETRAN was incorrect.[32,33] The effect is to decrease the surface dose and increase the dose near the end of the electron's range. This effect can be clearly observed in the dose point kernel of 1 MeV electrons shown in Fig. 11 comparing the results by Berger with the older ETRAN version[31] and the corrected results with the 1989 version of ETRAN (taken from Simpkin and Mackie[6]). These corrected results are in excellent agreement with the EGSnrc calculated values. There is a noticeable shift of the EGSnrc results deeper in the phantom compared to the EGS4 values which is caused by the inclusion of spin effects in the treatment of electron elastic scattering in EGSnrc. An EGSnrc calculation with spin effects turned off reproduces very well the EGS4 curve. As noted in Sec. 2.4.7.ii of the EGSnrc manual,[11] the effect of including spin effects is to make the effective range of electrons longer for low-Z materials.

III.C. Beta dose point kernels for polyenergetic sources

We have calculated the dose point kernel for two beta sources, ^{32}P and ^{90}Y, using spectra from ICRU Report 56.[19] Dose point kernels for ^{32}P and ^{90}Y beta particles were scaled by X_{90}, the sphere radius below which 90% of the emitted energy is absorbed in order to compare our results with values reported in the literature. Good agreement of the scaled dose kernels determined with EGSnrc can be observed in Fig. 12 with the EGS4 calculations by Simpkin and Mackie.[6] ETRAN calculations by Prestwitch *et al.*[34] and theoretical calculations by Berger based on Spencer theory of primary electron energy deposition[35] are also shown. The X_{90} value reported by Simpkin and Mackie[6] is shorter than ours. This can be caused by spin effects, which tend to make the effective range of the electrons longer for low-Z materials, and the use of different radial resolutions. While these authors used a 10 μm radial mesh, we used 5 and 1 μm for ^{32}P and ^{90}Y, respectively.

In Fig. 13 the dose rate per unit activity for a ^{32}P beta source is compared with the results from Janicki and Seuntjens[8] and Cross *et al.*[7] The first group of authors used their own EGSnrc user-code SPHERE_SCORE and the second authors used the ITS/ACCEPT code. The two EGSnrc calculations show excellent agreement. The results by Cross *et al.*[7] show significant discrepancies near the origin where they used the unrestricted collision stopping power approximation to estimate the dose at the origin.

IV. SUMMARY AND CONCLUSIONS

EGSnrc calculated energy depostion kernels for monoenergetic photons are different in some well-defined ways from those calculated earlier with EGS4/PRESTA. Binding effects reduce the number of Compton interactions increasing the amount of primary energy deposited per particle. The decrease in the number of Compton interactions directly affects the scatter component of these kernels. In previous calculations, Rayleigh scattering was not included, although we have shown that it reduces significantly the primary energy fraction and acts as a source of scattered photons, increasing the scatter component of the energy deposition kernel. The photo-electron angular sampling produces a redistribution of the energy deposited around the interaction site causing the backscattered energy fraction to increase up to 2.7 times for very low energy photons. Above the pair-production threshold the angular sampling of the electron–positron pair direction in EGSnrc produces a different angular profile of the primary dose to the one obtained by just using a fixed angle approximation as in EGS4. But at high energies, multiple scattering should "wash-out" any angular distribution of the energy depostion.

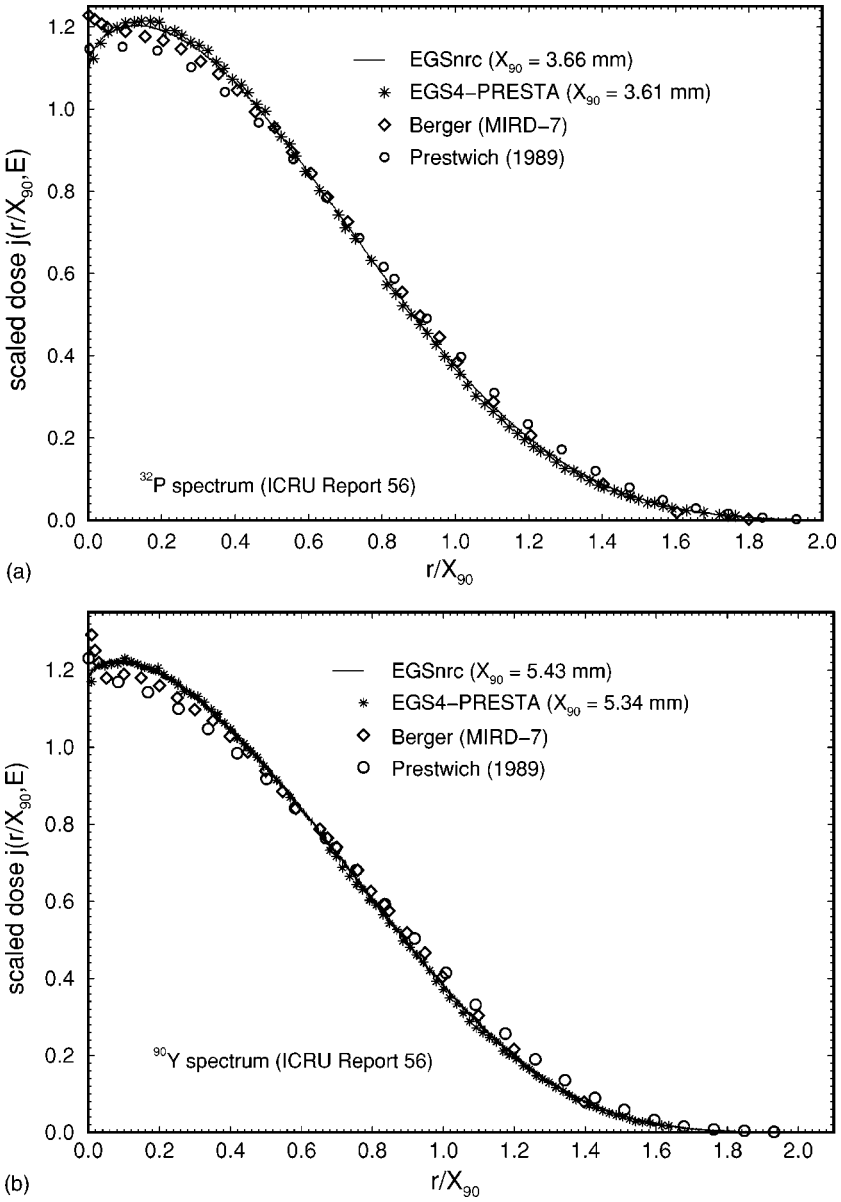

FIG. 12. Scaled dose kernels for ^{32}P and ^{90}Y beta particles determined with EGSnrc (solid line). EGS4 (stars) and ETRAN (circles) calculated values are shown for comparison together with theoretical calculations by Berger (diamonds). X_{90} is the radius of the water sphere inside of which 90% of the emitted energy is absorbed.

The primary energy fraction agrees very well with the ratio of the mass energy-absorption coefficients μ_{en} to the mass attenuation coefficient μ. All differences are less than or equal 0.5%. According to the small variation in the total energy fractions in the whole energy range studied (15 keV–50 MeV), which is less than 0.2%, both sets of kernels should give the same answer for broad beams incident on infinite homogeneous phantoms or equivalent conditions. In cases where one is interested in the dose near boundaries or interfaces these kernels might produce different results, especially in the diagnostic energy range. A study of the impact of the new kernels on the dose estimation using convolution based treatment planning systems in realistic situations is beyond the scope of this work but medical physicists are encouraged to undertake such a study.

The EGSnrc user-code EDKnrc has been shown to produce accurate dose point kernels which agree well with values calculated using EGS4/PRESTA at 50 and 100 keV. Differences in the results of both codes observed at 1 MeV can be attributed to the inclusion in EGSnrc of spin effects in the treatment of electron scattering. At 1 MeV, the EGSnrc scaled dose distribution agrees well with ETRAN calculations obtained with the corrected version of this code. Moreover, radial dose rate distributions for ^{32}P and ^{90}Y beta sources calculated with our code have been compared with results obtained with an independent EGSnrc user-code were found to be in excellent agreement. The EDKnrc user-code is being distributed with the EGSnrc system.[14]

ACKNOWLEDGMENTS

The authors gratefully acknowledge contribution of low energy deposition kernels from Dr. Parham Alaei. Many thanks to Dr. Jan Seuntjens and Dr. Christian Janicki who provided us with their beta kernels at an early stage of their work.

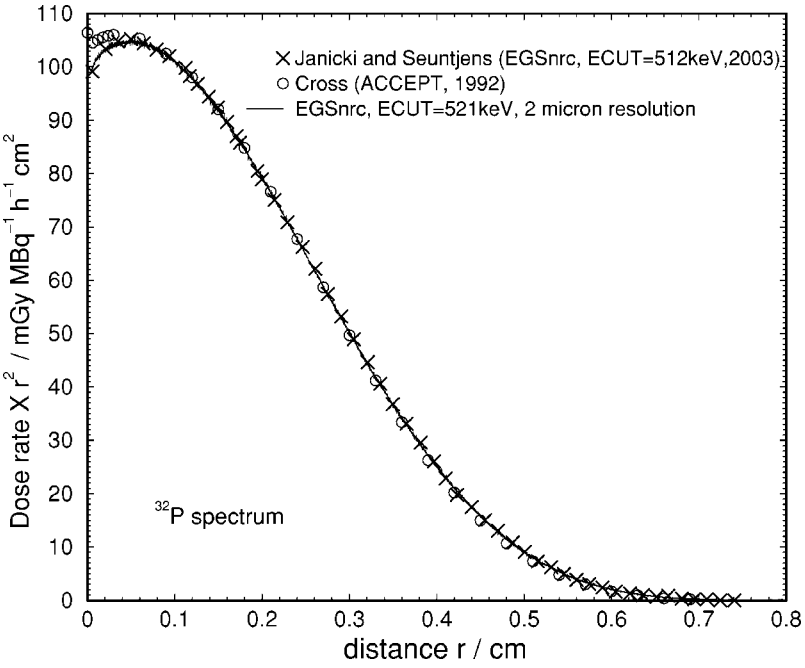

FIG. 13. Dose rate in water per unit activity times the distance squared from a ^{32}P beta spectrum as calculated with EDKnrc and compared with the recent calculations by Janicki and Seuntjens (Ref. 8) using their EGSnrc user-code SPHERE_SCORE and the calculations by Cross with ACCEPT from the ITS series of codes (Ref. 36).

[a]Electronic mail: mainegra@irs.phy.nrc.ca

[1]T. R. Mackie, J. W. Scrimger, and J. J. Battista, "A convolution method of calculating dose for 15 MV x-rays," Med. Phys. **12**, 188–196 (1985).
[2]T. R. Mackie, A. F. Bielajew, D. W. O. Rogers, and J. J. Battista, "Generation of photon dose spread arrays using the EGS4 Monte Carlo code," Med. Phys. **12**, 515 (1985).
[3]R. Mohan, C. Chui, and L. Lidofsky, "Differential pencil beam dose computation model for photons," Med. Phys. **13**, 64–73 (1986).
[4]A. Ahnesjö, P. Andreo, and A. Brahme, "Calculation and application of point spread functions for treatment planning with high energy photon beams," Acta Oncol. **26**, 49–57 (1987).
[5]T. R. Mackie, A. F. Bielajew, D. W. O. Rogers, and J. J. Battista, "Generation of energy deposition kernels using the EGS Monte Carlo code," Phys. Med. Biol. **33**, 1–20 (1988).
[6]D. J. Simpkin and T. R. Mackie, "EGS4 Monte Carlo determination of the beta dose kernel in water," Med. Phys. **17**, 179–186 (1990).
[7]W. G. Cross, N. Freedman, and P. Y. Wong, "Beta-ray dose distributions from point sources in an infinite water medium," Phys. Med. Biol. **63**, 160–171 (1992).
[8]C. Janicki and J. Seuntjens, "Re-evaluation of the dose to the cyst wall in P-32 radiocolloid treatments of cystic brain tumors using the Dose-Point-Kernel and Monte Carlo methods," Med. Phys. **30**, 2475–2481 (2003).
[9]C. Janicki and J. Seuntjens, "Accurate determination of dose-point-kernel functions close to the origin using Monte Carlo simulations," Med. Phys. **31**, 814–818 (2004).
[10]A. Ahnesjö and P. Andreo, "Determination of effective bremsstrahlung spectra and electron contamination for photon dose calculations," Phys. Med. Biol. **34**, 1451–1464 (1989).
[11]I. Kawrakow and D. W. O. Rogers, "The EGSnrc Code System: Monte Carlo simulation of electron and photon transport," Technical Report PIRS-701, National Research Council of Canada, Ottawa, Canada, 2000 (see http://www.irs.inms.nrc.ca/inms/irs/EGSnrc/EGSnrc.html).
[12]I. Kawrakow, "Accurate condensed history Monte Carlo simulation of electron transport. I. EGSnrc, the new EGS4 version," Med. Phys. **27**, 485–498 (2000).
[13]P. Alaei, B. J. Gerbi, and R. A. Geise, "Generation and use of photon energy deposition kernels for diagnostic quality x rays," Med. Phys. **26**, 1687–1697 (1999).
[14]D. W. O. Rogers, I. Kawrakow, J. P. Seuntjens, B. R. B. Walters, and E. Mainegra-Hing, "NRC User Codes for EGSnrc," Technical Report PIRS-702(RevB), National Research Council of Canada, Ottawa, Canada, 2003.
[15]B. R. B. Walters, I. Kawrakow, and D. W. O. Rogers, "History by history statistical estimators in the BEAM code system," Med. Phys. **29**, 2745–2752 (2002).
[16]M. J. Berger and J. H. Hubbell, "XCOM: Photon Cross Sections on a Personal Computer," Report NBSIR87-3597, NIST, Gaithersburg, MD20899, 1987.
[17]F. Hobeila and J. P. Seuntjens, "Effect of XCOM photoelectric cross-sections on dosimetric quantities calculated with EGSnrc, IAEA-CN-96/17P," in *Proceedings of the International Symposium on Standards and Codes of Practice in Medical Radiation Dosimetry* (IAEA, Vienna, 2003), Vol. **1**, pp. 177–186.
[18]J. P. Seuntjens, I. Kawrakow, J. Borg, F. Hobeila, and D. W. O. Rogers, "Calculated and measured air-kerma response of ionization chambers in low and medium energy photon beams," in *Recent Developments in Accurate Radiation Dosimetry, Proceedings of an International Workshop*, edited by J. P. Seuntjens and P. Mobit (Medical Physics, Madison WI, 2002), pp. 69–84.
[19]ICRU, "Dosimetry of external beta rays for radiation protection," ICRU Report 56, ICRU, Washington, DC, 1997.
[20]ICRU, "Stopping powers for electrons and positrons," ICRU Report 37, ICRU, Washington, DC, 1984.
[21]H. W. Koch and J. W. Motz, "Bremsstrahlung cross-section formulas and related data," Rev. Mod. Phys. **31**, 920–955 (1959).
[22]D. W. O. Rogers, S. Duane, A. F. Bielajew, and W. R. Nelson, "Use of ICRU-37/NBS radiative stopping powers in the EGS4 system," National Research Council of Canada report PIRS-0177, 1989.
[23]E. Storm and H. I. Israel, "Photon cross sections from 1 keV to 100 MeV for elements $Z=1$ to $Z=100$," At. Data Nucl. Data Tables **7**, 565–681 (1970).
[24]J. H. Hubbell, "Photon cross sections, attenuation coefficients, and energy absorption coefficients from 10 keV to 100 GeV," NBS Report NSRDS-NBS 29, 1969).
[25]J. H. Hubbell, "Photon mass attenuation coefficients and mass energy-absorption coefficients for H, C, N, O, Ar, and seven mixtures from 0.1 keV to 20 MeV," Radiat. Res. **70**, 58–81 (1977).
[26]J. H. Hubbell, "Photon mass attenuation and energy-absorption coefficients from 1 keV to 20 MeV," Int. J. Appl. Radiat. Isot. **33**, 1269–1290 (1982).
[27]C. E. de Almeida, A. J. Pereira, M. H. Marechal, G. Pereira, J. C. Cruz, J. C. Ferraz, A. J. Giordani, C. M. Khalil, R. M. Martins, G. Menegussi, D. Moreira, J. R. Rocha, and M. A. Pinto, "Intercomparison of calibration procedures for ^{192}Ir HDR sources in Brazil," Phys. Med. Biol. **44**, N31–N38 (1999).
[28]J. H. Hubbell and S. M. Seltzer, "Tables of x-ray mass attenuation coefficients and mass energy-absorption coefficients 1 keV to 20 MeV for elements $Z=1$ to 92 and 48 additional substances of dosimetric interest," technical Report NISTIR 5632, NIST, Gaithersburg, MD, 1995.

[29]F. Sauter, "Über den atomaren Photoeffekt in der K-Schale nach der relativistischen Wellenmechanik Diracs," Ann. Phys. **11**, 454–488 (1931).
[30]A. F. Bielajew and D. W. O. Rogers, "Photoelectron angular distribution in the EGS4 code system," National Research Council of Canada Report PIRS-0058, 1986.
[31]M. J. Berger, "Improved point kernels for electron and beta ray dosimetry," NBS Report NBSIR 73-107, 1973.
[32]D. W. O. Rogers and A. F. Bielajew, "Differences in electron depth dose curves calculated with EGS and ETRAN and improved energy range relationships," Med. Phys. **13**, 687–694 (1986).
[33]S. M. Seltzer, "An overview of ETRAN Monte Carlo methods," in *Monte Carlo Transport of Electrons and Photons*, edited by T. M. Jenkins, W. R. Nelson, A. Rindi, A. E. Nahum, and D. W. O. Rogers (Plenum, New York, 1988), pp. 153–182.
[34]W. V. Prestwich, J. Nunes, and C. S. Kwok, "Beta dose point kernels for radionuclides of potential use in radioimmunotherapy," J. Nucl. Med. **30**, 1036–1046 (1989).
[35]M. J. Berger, "Distribution of absorbed dose around point sources of electrons and beta particles in water and other media," (MIRD Pamphlet No. 7) J. Nucl. Med. **12**, 5–24 (1971).
[36]J. A. Halbleib and T. A. Mehlhorn, "ITS: The integrated TIGER series of coupled electron/photon Monte Carlo transport codes," Sandia Report SAND84-0573, 1984.